THE JOURNAL OF PHYSICAL CHEMISTRY A

Article

pubs.acs.org/JPCA

IRMPD Spectroscopy of Metalated Flavins: Structure and Bonding of Lumiflavin Complexes with Alkali and Coinage Metal Ions

Pablo Nieto,[†] Alan Günther,[†] Giel Berden,[#] Jos Oomens,[#,‡] and Otto Dopfer*[,†]

[†]Institut für Optik und Atomare Physik, Technische Universität Berlin, Hardenbergstrasse 36, D-10623 Berlin, Germany

[#]Radboud University, Institute for Molecules and Materials, FELIX Laboratory, Toernooiveld 7c, 6525 ED Nijmegen, The Netherlands

[‡]van't Hoff Institute for Molecular Sciences, University of Amsterdam, Science Park 904, 1098XH Amsterdam, The Netherlands

Supporting Information

ABSTRACT: Flavins are a fundamental class of biomolecules, whose photochemical properties strongly depend on their environment and their redox and metalation state. Infrared multiphoton dissociation (IRMPD) spectra of mass-selected isolated metal−lumiflavin ionic complexes (M^+LF) are analyzed in the fingerprint range (800−1830 cm^{-1}) to determine the bonding of lumiflavin with alkali (M = Li, Na, K, Cs) and coinage (M = Cu, Ag) metal ions. The complexes are generated in an electrospray ionization source coupled to an ion cyclotron resonance mass spectrometer and the IR free electron laser FELIX. Vibrational and isomer assignments of the IRMPD spectra are accomplished by comparison to quantum chemical calculations at the B3LYP/cc-pVDZ level, yielding structure, binding energy, bonding mechanism, and spectral properties of the complexes. The most stable binding sites identified in the experiments involve metal bonding to the oxygen atoms of the two available CO groups of LF. Hence, CO stretching frequencies are a sensitive indicator of both the metal binding site and the metal bond strength. More than one isomer is observed for M = Li, Na, and K, and the preferred CO binding site changes with the size of the alkali ion. For Cs^+LF, only one isomer is identified, although the energies of the two most stable structures differ by less than 7 kJ/mol. While the M^+−LF bonds for alkali ions are mainly based on electrostatic forces, substantial covalent contributions lead to stronger bonds for the coinage metal ions. Comparison between lumiflavin and lumichrome reveals substantial differences in the metal binding motifs and interactions due to the different flavin structures.

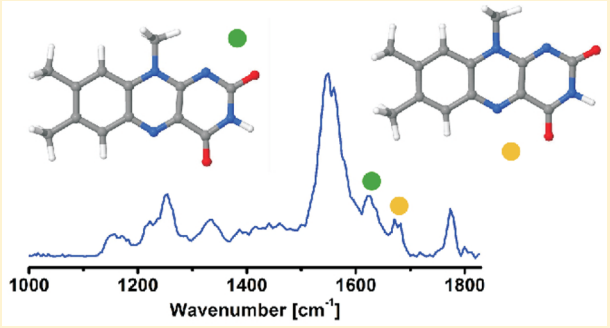

1. INTRODUCTION

Flavins (Fls) are a large class of biomolecules derived from the 7,8-dimethyl-10-alkylisoalloxazine chromophore (*iso*-lumichrome, *iso*-LC for R = H), which differ by their substituents at the N10 position and play a key role in many biochemical processes.[1,2] The most important examples of the Fl family are lumichrome (LC), lumiflavin (LF, Figure 1), riboflavin (RF, vitamin B_2), flavin mononucleotide (FMN), and flavin adenosine dinucleotide (FAD). Their diverse (photo)chemical properties make them of fundamental importance for many biological systems and phenomena. Their relevance was acknowledged by the Nobel Prize in Chemistry awarded to Paul Karrer in 1937 for his work on Fls and vitamins. Fls absorb in a wide spectral range from the optical to the UV region, and their spectroscopic properties vary sensitively with their oxidation, protonation, metalation, and solvation state.[2−8] In this way, Fl-containing domains act as light-harvesting modules in plants and algal phototropins and as blue light receptors in fungals.[9,10] Moreover, as important components of flavoproteins, they occur as catalysts in the oxidation of glucose by GOx enzymes and in the repair of DNA,[11] and they are involved as electron donors and acceptors in the redox cycle of the respiratory chain.[12]

The complexation of Fls with metal ions is of particular interest because the additional charge has an important effect on their electronic and redox properties, which is signaled by large shifts in their absorption spectra.[13] Optical excitation in Fls is primarily provided by n → π^* and π→ π^* transitions.[1,2] Metal cations can bind to the aromatic chromophore via π-stacking or to nucleophilic N and O centers via σ-bonding. Thus, they substantially modify the electronic structure of both the $\pi^{(*)}$ and n orbitals, which in turn can drastically change the photochemistry of the Fl chromophore. The broad majority of the studies of metal−Fl cation complexes were carried out in solution.[3−8] Unfortunately, the considerable influence of solvent and counterions is not yet fully understood. Hence, spectroscopic studies on isolated Fl molecules and their aggregates are crucial to provide information about the structural, electronic, and chemical properties of the optically

Received: August 16, 2016
Revised: October 1, 2016
Published: October 1, 2016

DOI: 10.1021/acs.jpca.6b08281
J. Phys. Chem. A 2016, 120, 8297−8308

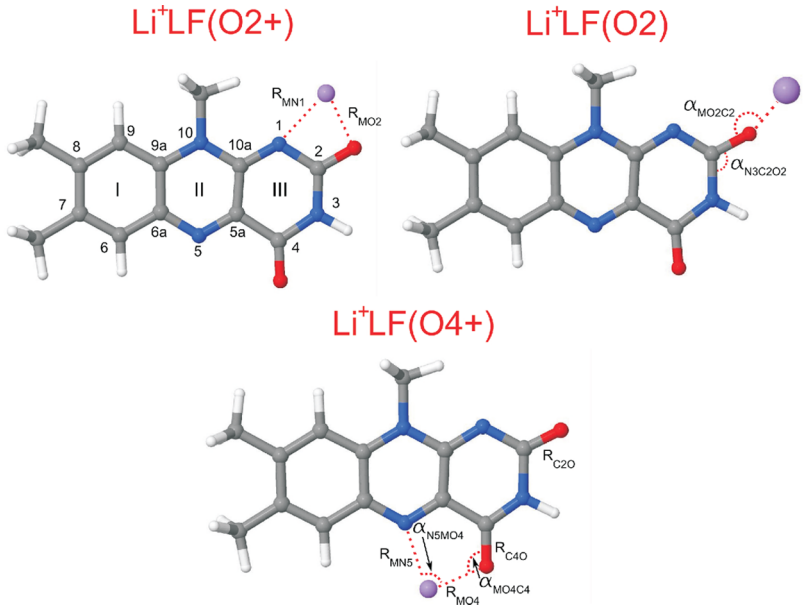

Figure 1. Structures of the planar O4+, O2+, and O2 isomers of M^+LF complexes with alkali cations illustrated for M = Li, including the atomic and ring numbering (according to IUPAC) and relevant structural parameters.

active species and to disentangle the individual effects of metalation and solvation. To reach this goal, basic properties of Fls, such as their geometric and electronic structure, stability, and interaction with metal ions and solvent must be characterized at the molecular level.[14,15] However, due to their difficult preparation in the gas phase, experiments on isolated Fls have been rather scarce,[14,16−18] and studies of their metal and solvent adducts have been completely lacking until recently.[15] The few available studies include a fluorescence spectrum of LC embedded in superfluid He droplets,[17] the determination of the proton affinity of LF by mass spectrometry,[16] and the photo- and collision-induced fragmentation of protonated FMN.[18] In addition, the preferred protonation sites of several isolated protonated Fls, including LC, LF, RF, and FMN, have recently been determined by infrared multiphoton dissociation (IRMPD) spectroscopy and quantum chemical calculations.[14] It was found that the protonation site strongly depends on the Fl substituent and that the strongly IR active CO stretch modes can be used to identify the protonation site. A subsequent investigation extended these IRMPD studies to M^{q+}LC complexes with the closed-shell metal ions M^{q+} = Li^+−Cs^+, Ag^+, and Mg^{2+} (i.e., Mg^+−LC_2), using the same experimental and computational protocol.[15] Systematic analysis of M^+LC within the series of the alkali ions (Li−Cs) reveals the effects of the size of the metal ion on the preferred binding site, the metal binding energy, and the bonding mechanism, which turns out to be mostly electrostatic in nature. Substantial additional covalent contributions to the chemical bonding mechanism in Ag^+LC result from the electronic configuration of the Ag coinage transition metal, which undergoes $d^{10-x}s^x$ hybridization upon complex formation.

In the present work, we extend these M^+LC studies to M^+LF complexes with alkali (Li−Cs) and coinage (Cu, Ag, Au) metal ions to determine the effects of the additional methyl group at N10 and the lacking H atom at N1 on the preference for the various metal binding motifs. Similarly to M^+LC, the preferred binding sites in M^+LF are the O4 and the O2 atoms of the two available CO groups. Therefore, the two CO stretch vibrations can again be used as indicators for the presence of different isomers. The comparison of the measured IRMPD spectra with quantum chemical calculations provides deeper understanding of the bonding mechanisms and structures. The employed combined approach of IRMPD spectroscopy and DFT calculations has extensively been applied to protonated and metalated aromatic and biological molecules to determine their geometric and energetic properties.[14,15,19−46]

2. EXPERIMENTAL AND COMPUTATIONAL TECHNIQUES

IRMPD spectra of M^+LF complexes with M = Li, Na, K, Cs, Cu, and Ag are recorded in the 800−1830 cm^{-1} range in a Fourier-transform ion cyclotron resonance mass spectrometer (FT-ICR-MS)[47] coupled to an electrospray ionization source and the IR beamline of the Free Electron Laser for Infrared eXperiments (FELIX).[34,48,49] LF (>99%) purchased from Sigma-Aldrich is used without further purification. The metal complexes are produced by mixing a 0.2 mM solution of LF dissolved in methanol with concentrations of metal chloride salt solutions in water in the 1−6 mM range. Typically, a proportion of eight parts of methanol and one part of water is used. The solutions are then sprayed at a flow rate of 10 μL/min. The generated M^+LF complexes are accumulated in a hexapole ion trap and transferred via an octopole ion guide into the ICR cell. In the ICR trap, the ions of interest are mass-selected and irradiated with 15−25 macropulses from FELIX operating at a repetition rate of 10 Hz. The typical macropulse energy is measured as 20−65 mJ and is attenuated for weakly bound clusters (such as Cs^+LF) in order to prevent saturation effects (i.e., complete depletion). The bandwidth of the FELIX radiation is about 0.5% fwhm of the central wavelength. Calibration of the wavelength with an accuracy of ±0.02 μm is achieved by a grating spectrometer. Depending on the scanned frequency range, the laser step size varies between 3 and 8 cm^{-1}. Parent and fragment ion intensities, I_P and I_F, are monitored as a function of the laser frequency, and the IRMPD yield is determined as $I_{IRMPD} = I_F/(I_P + I_F)$. The monitored

DOI: 10.1021/acs.jpca.6b08281
J. Phys. Chem. A 2016, 120, 8297−8308

Table 1. Binding and Relative (Free) Energies (kJ/mol) Calculated for Different M^+LF Isomers at the B3LYP/cc-pVDZ Level[a]

alkali metal	ΔG	ΔE	coinage metal	ΔG	ΔE
Li^+LF(O4+)	**0.0 (−276.9)**	**0.0 (−308.6)**	**Cu^+LF(O4+)**	**0.0 (−350.2)**	**0.0 (−385.1)**
Li^+LF(O2+)	+7.2	+11.9	Cu^+LF(O2+)	+26.3	+30.5
Li^+LF(O2)	+16.0	+20.0	Cu^+LF(O2−)	+50.7	+55.3
Li^+LF(I)	+183.2	+185.4	Cu^+LF(O4−)	+75.6	+79.5
Li^+LF(N10)	+221.9	+228.6	Cu^+LF(I)	+164.1	+167.9
Na^+LF(O4+)	**0.0 (−194.5)**	**0.0 (−226.1)**	**Ag^+LF(O4+)**	**0.0 (−262.1)**	**0.0 (−295.9)**
Na^+LF(O2+)	+3.9	+7.2	Ag^+LF(O2+)	+3.0	+12.6
Na^+LF(O2)	+6.3	+11.4	Ag^+LF(O2−)	+37.9	+43.3
Na^+LF(I)	+154.6	+159.6	Ag^+LF(O4−)	+59.6	+63.7
K^+LF(O2)	**0.0 (−153.7)**	**0.0 (−180.7)**	Ag^+LF(I)	+151.3	+155.0
K^+LF(O2+)	+0.4	+1.7	**Au^+LF(O4+)**	**0.0 (−320.8)**	**0.0 (−354.9)**
K^+LF(O4+)	+3.4	+0.5	Au^+LF(O2+)	+1.8	+3.9
Rb^+LF(O2)	**0.0 (−134.7)**	**0.0 (−161.5)**	Au^+LF(O2−)	+26.6	+28.8
Rb^+LF(O4+)	+4.8	+2.1	Au^+LF(O4−)	+51.8	+54.1
Cs^+LF(O2)	**0.0 (−121.6)**	**0.0 (−148.2)**	Au^+LF(I)	+123.0	+127.0
Cs^+LF(O4+)	+6.5	+2.4			

[a]Absolute (free) energies are given for the global minima, while relative energies are listed for the local minima.

fragments are given in Table S1 in the Supporting Information (SI). As the IRMPD spectra are similar for individual isotopes of M, they are averaged. Finally, the IRMPD yield is linearly normalized for the frequency-dependent variations in the laser power (Figure S1 in the SI).

Density functional theory calculations at the B3LYP/cc-pVDZ level are carried out for the monoisotopic masses of M^+LF using GAUSSIAN09.[50] Relativistic corrections for the heavier metal cations (K−Cs, Cu−Au) are included using the Stuttgart VDZ effective core potentials (ECPs).[51] Previous studies on H^+Fl and M^{q+}LC clearly show that the results at the B3LYP/cc-pVDZ level are quantitatively very close to those obtained with larger basis sets and MP2 calculations.[14,15] Furthermore, the B3LYP/cc-pVDZ level reproduces reasonably well both frequencies and relative IR intensities of the measured transitions. Calculated harmonic vibrational frequencies of M^+Fl are scaled by factors of 0.964 (Li, Na) and 0.973 (K−Cs, Cu−Au), as previously derived for M^{q+}LC.[14] All energies are corrected for harmonic zero-point vibrational energies. Binding energies (E) and Gibbs free energies (G) evaluated at room temperature (298 K) are computed for all complexes. Calculated linear IR absorption stick spectra are convoluted with a Gaussian profile using a fwhm of 20 cm^{-1} to facilitate convenient comparison with the experimental IRMPD spectra. At this stage, one should recall that IRMPD relies on multiple-photon absorption and subsequent dissociation, which may cause modest red shifts and intensity modifications compared to a (measured and calculated) single-photon linear IR absorption spectrum.[14,34,52] Charge distributions are determined with the Natural Bonding Orbital (NBO) method.[53]

3. RESULTS AND DISCUSSION

A variety of metal binding sites are considered for each M^+LF complex. M^+ may attach to the nucleophilic LF binding sites (Figure 1), such as the lone pairs of the O atoms of the two CO groups (denoted O2 and O4), the lone pairs of the two heterocyclic N atoms (N1 and N5), and the π electrons of the aromatic rings (I−III). A further stable out-of-plane binding site is found at N10. For the O2 (O4) isomers, the notation + or − indicates the orientation of M^+ with respect to N3. When M^+ is located away from N3, it is assigned as O2+ (O4+), whereas the opposite configuration is denoted O2− (O4−). No sign is given when the C═O−M bonds are approximately collinear. Calculated binding energies and Gibbs free energies for all isomers are summarized in Table 1. Although no experiments have been carried out for Rb^+LF and Au^+LF, their structures are also calculated for completeness. The results for the alkali ions will be discussed first, followed by those for the coinage metal ions.

3.1. M^+LF with M = Li−Cs. The IRMPD spectra obtained for all considered M^+LF complexes are compared in Figure 2 with that of H^+LF reported previously.[14] The predominant

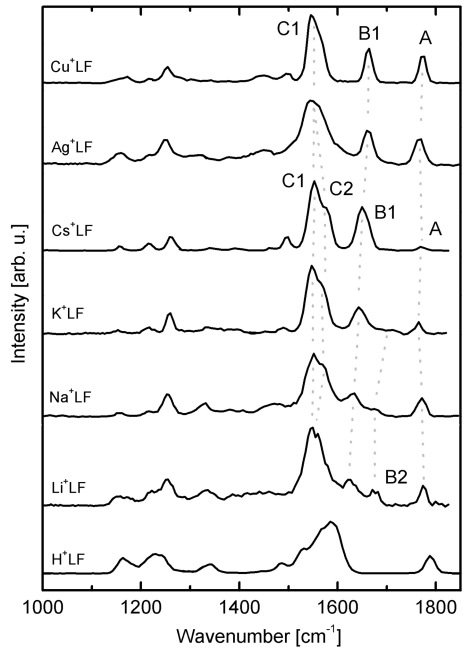

Figure 2. IRMPD spectra of M^+LF with M = Li, Na, K, Cs, Ag, and Cu recorded in the fingerprint range. For comparison, the spectrum of H^+LF is shown as well.[14] Corresponding transitions assigned to the free and bound CO stretch modes (A, B1, and B2) and the intense ring C−C/C−N stretch modes (C1, C2) are connected by dotted lines. The positions of the transitions observed are listed in Table 2, along with vibrational and isomer assignments.

DOI: 10.1021/acs.jpca.6b08281
J. Phys. Chem. A 2016, 120, 8297−8308

doublet in the 1520−1580 cm^{-1} range (labeled C1 and C2) is assigned to coupled C−C/C−N ring stretch modes, denoted ν_{CN} and ν_{CN}'. The doublet is clearly resolved for Na, K, and Cs, while for Li, the C2 shoulder is not resolved. The splitting between C1 and C2 (22−25 cm^{-1}) does not depend much on M^+. Three further peaks labeled A, B1, and B2 occur in the 1600−1800 cm^{-1} range and are assigned to the two CO stretch modes of the various isomers. The spectral variations of all five peaks (A, B1, B2, C1, and C2) are indicative of the various isomers present in the experiment and allow for the discrimination of different metal binding sites, as demonstrated in previous studies on H^+Fl and M^{q+}LC.[14,15] The positions of their maxima are summarized in Table 2 along with their vibrational and isomer assignments. Band A, located at around 1770 cm^{-1} and assigned to the free CO stretch mode, slightly shifts to lower frequencies from Li to K. It also varies in relative intensity with higher alkali mass, possibly because of a significant drop in laser power in this spectral range toward higher frequency (Figure S1 in the SI). Band B1 attributed to a bound CO stretch is observed at 1627 cm^{-1} for Li and shifts toward higher frequencies with larger alkali mass up to 1652 cm^{-1} for Cs. A second and less pronounced peak labeled B2, assigned to the bound CO stretch of a second isomer, is observed for Li−K (1675−1702 cm^{-1}) but is not detected for Cs.

Table 2. Maxima (cm^{-1}) of the Three Dominant Bands A−C Observed in the IRMPD Spectra of M^+LF (Figure 2) along with Their Major Vibrational and Isomer Assignments

	position[a]	assignment
Li^+LF	1775 ± 6 (A)	ν_{C2O}(O4+)/ν_{C4O}(O2(+))
	1675 ± 6 (B2)	ν_{C4O}(O4+)
	1627 ± 6 (B1)	ν_{C2O}(O2(+))
	1552 ± 5 (C1)	ν_{CN}(O4+/O2(+))
Na^+LF	1771 ± 6 (A)	ν_{C2O}(O4+)/ν_{C4O}(O2(+))
	1676 ± 6 (B2)	ν_{C4O}(O4+)
	1631 ± 5 (B1)	ν_{C2O}(O2(+))
	1573 ± 5 (C2)	ν_{CN}(O4+)
	1548 ± 5 (C1)	ν_{CN}'(O2(+))
K^+LF	1765 ± 7 (A)	ν_{C2O}(O4+)/ν_{C4O}(O2(+))
	1702 ± 13 (B2)	ν_{C4O}(O4+)
	1644 ± 5 (B1)	ν_{C2O}(O2(+))
	1569 ± 5 (C2)	ν_{CN}(O2(+))
	1547 ± 5 (C1)	ν_{CN}'(O4+)
Cs^+LF	1776 ± 12 (A)	ν_{C4O}(O2)
	1652 ± 6 (B1)	ν_{C2O}(O2)
	1577 ± 5 (C2)	ν_{CN}(O2)
	1552 ± 5 (C1)	ν_{CN}'(O2)
Ag^+LF	1766 ± 6 (A)	ν_{C2O}(O4+)
	1662 ± 6 (B1)	ν_{C4O}(O4+)
	1552 ± 5 (C1)	ν_{CN}(O4+)
Cu^+LF	1773 ± 6 (A)	ν_{C2O}(O4+)
	1663 ± 6 (B1)	ν_{C4O}(O4+)
	1552 ± 5 (C1)	ν_{CN}(O4+)

[a]The errors are taken from the least-squares fits to Gaussian functions and the wavelength calibration error.

A detailed search on the Li^+LF potential energy surface at the B3LYP/cc-pVDZ level results in five nonequivalent minima. Three of them are formed by strong σ-bonds of Li^+ at the O4+, O2+, and O2 sites with binding free energies of 277, 270, and 261 kJ/mol, respectively (Figure 1). Two much less stable π-bonded isomers, namely, I and N10, have much lower binding energies of 94 and 55 kJ/mol, respectively (Figure S2 in the SI). It is straightforward to understand the comparatively high binding energy of O4+ and O2(+) with respect to I and N10 by taking into account the strong electrostatic interaction between the M^+ cations and the negatively charged, nucleophilic O4 and O2 atoms. Only the linear IR absorption spectra predicted for the O2(+) and O4+ isomers of Li^+LF match the experimental IRMPD spectrum (Figure S3 in the SI). The π-isomers feature two intense free CO stretch bands in the 1750 cm^{-1} range (in disagreement with experiment) and can also be discarded on the basis of their relative free energies. The same conclusions apply to the other M^+LF complexes investigated here. Hence, in the following, we consider only the O2 and O4 binding motifs for further analysis. The linear IR spectra calculated for the three lowest-energy structures of M^+LF, along with their relative free energies, are compared in Figure 3 to their IRMPD spectra for M = Li−K and Cs. Corresponding calculated spectra for M = Rb are available in Figure S5 in the SI. Comparison between the measured and calculated IR spectra suggests that the B1 and B2 transitions are assigned to bound CO stretch modes, namely, to the C2O stretch of the O2(+) isomers (B1) and the C4O stretch of the O4+ isomers (B2). Bands A are assigned to the corresponding free CO stretch modes, namely, the C2O stretch of O4+ and the C4O stretch of O2(+). Relevant structural, vibrational, and energetic properties as well as the charge distributions of the O4+ and O2(+) isomers of all M^+LF complexes considered are summarized in Tables 1 and 3−5 and are visualized in Figures S9−S11 in the SI as a function of the inverse radius of M^+ ($1/R_M$).

The planar O4+ isomer with C_s symmetry, in which M^+ binds in a chelate configuration to the lone pairs of both O4 and N5, is the most stable M^+LF structure for the lighter alkali ions Li^+ and Na^+. The binding energies (E) of O4+ decrease with the size of M^+ from 309 (Li) to 146 kJ/mol (Cs), and the free energies follow the same trend (G = 277−115 kJ/mol). According to the increasing ionic radius (R_M = 0.76−1.67 Å for Li−Cs) and decreasing interaction energy (Table 1), the bond lengths of M^+ to the O4 and N5 atoms increase with the size of M^+ (R_{MO4} = 1.84−2.77 Å, R_{MN5} = 2.09−3.40 Å; Table 3). Because the equilibrium position of M^+ is further away from O4 and N5 for increasing ion size, the chelate angle α_{N5MO4} decreases (87.8−52.8°), while the angle α_{MO4C4} opens up (110.8−134.4°). Because the M^+−O4 bond is stronger and shorter than the M^+−N5 bond, the N5−M−O4 chelate is quite asymmetric. Only modest charge transfer from M^+ to LF is expected because the ionization energies of the alkali metals (IE = 5.39−3.89 eV for Li−Cs)[54] are much lower than that of LF (calculated as IE = 7.72 eV). Indeed, our calculations predict a small charge transfer from M^+ to LF, which increases from Cs to Li ($-\Delta q_M$ = 85−128 me; Table 4), in line with the stronger and shorter bonds. Metalation of LF at O4 results not only in significant charge rearrangements on N5 and O4 ($-\Delta q_{N5}$ = 67−143 me, $-\Delta q_{O4}$ = 149−163 me; Table 4) but also slightly affects the remote C2O group (Δq_{O2} = 44−63 me). The interaction with M^+ causes a substantial elongation of the C4O bond and a strong red shift of the corresponding IR-active stretch mode (ΔR_{C4O} = 2.4−3.6 pm, $-\Delta\nu_{C4O}$ = 58−79 cm^{-1}). Due to conjugation through the pyrimidine ring, the free C2O bond contracts ($-\Delta R_{C2O}$ = 0.7−1.0 pm) and the corresponding vibration is blue-shifted ($\Delta\nu_{C2O}$ = 40−32 cm^{-1}). These trends are similar to those previously observed for the O4+ isomers of M^+LC.[15]

DOI: 10.1021/acs.jpca.6b08281
J. Phys. Chem. A 2016, 120, 8297−8308

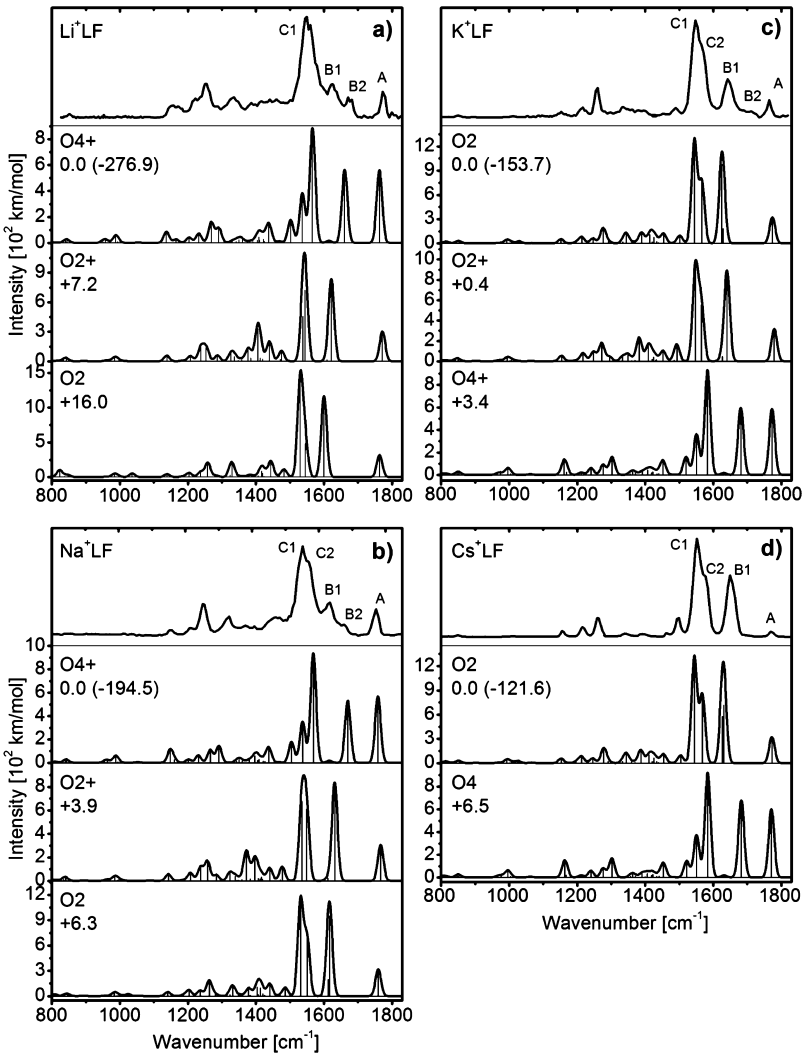

Figure 3. Experimental IRMPD spectra of M^+LF complexes with the alkali metals M = Li (a), Na (b), K (c), and Cs (d) compared to linear IR absorption spectra calculated for the lowest-energy isomers (B3LYP/cc-pVDZ). Calculated stick spectra are convoluted with a Gaussian line profile with fwhm = 20 cm^{-1}. Relative (absolute) free energies for the global (local) minima are given in kJ/mol.

The two planar O2-type isomers of M^+LF (C_s) with M^+ binding to the C2O carbonyl group of LF, namely, the O2+ chelate (N1−M−O2) and the O2 isomer with linear C2═O−M configuration, are less stable local minima than the global minima for the small alkali metals Li and Na. However, for K−Cs, the O2 isomers of M^+LF become the global minima. The energy difference between the most stable Li^+LF(O4+) and the second most stable Li^+LF(O2+) isomer is calculated as ΔE = 11.9 kJ/mol (ΔG = 7.2 kJ/mol). All three O4+ and O2(+) isomers differ only by ΔE = 1.7 kJ/mol (ΔG = 3.4 kJ/mol) for K^+LF. The O2+ chelate isomer of M^+LF is not found to be stable for alkali ions larger than K, possibly due to the repulsive interaction between the methyl group and M^+. Hence, the O2(+) bonding preference changes sensitively with the size of the M^+ ion and can be rationalized in the following way. In the absence of a nearby N atom (with its lone pair), M^+ strongly prefers a linear approach to the C2O group, and this O2 configuration is indeed favored for K−Cs. In addition to the interaction with O2, the smaller alkali ions can benefit from the interaction with the N1 lone pair, leading to the preferential formation of the O2+ chelate. Despite similar binding energies, the M−O2 bonds in the O2 isomers (R_{MO2} = 1.72−2.39 Å for M = Li−K) are substantially shorter than those of the O2+ isomers (R_{MO2} = 1.85−2.46 Å), suggesting that they are stronger in the linear C2═O−M configuration. On the other hand, the M−O2 bonds in the O2+ isomers are similar to the M−O4 bonds in the O4+ isomers (R_{MO4} = 1.84−2.48 Å for M = Li−K), in line with the comparable stabilization energies for the O2+ and O4+ chelates. This observation indicates that the additional M−N5 (O4+) and the M−N1 (O2+) interaction can provide a slight net stabilization of M^+LF. The total charge transfer from M^+ to LF is highest for the O4+ ($-\Delta q_M$ = 84−128 me for M = Li−K) and O2+ isomers ($-\Delta q_M$ = 70−120 me) and is lower for the O2 isomer ($-\Delta q_M$ = 54−77 me for M = Li−K). Not surprisingly, metalation at O2 has a strong impact on the C2O bond length and stretch frequency, and this effect is stronger for the linear O2 isomers (ΔR_{C2O} = 3.8−5.2 pm, $-\Delta\nu_{C2O}$ = 106−131 cm^{-1} for M = Li−K) than that for the O2+ chelate structures (ΔR_{C2O} = 3.0−3.7 pm, $-\Delta\nu_{C2O}$ = 91−110 cm^{-1}) due to the stronger M−O2 bonds in the former complexes. By conjugation through the pyrimidine ring, also the free C4O bond in O2 (O2+) is slightly affected by metalation at the O2 site, with a contraction of $-\Delta R_{C4O}$ = 0.6−0.8 pm (0.8−1.1 pm) and a corresponding blue shift of $\Delta\nu_{C4O}$

DOI: 10.1021/acs.jpca.6b08281
J. Phys. Chem. A 2016, 120, 8297−8308

Table 3. Bond Lengths and Angles (Å, degrees) and Scaled CO Stretch Frequencies (cm^{-1}) of M^+LF Calculated at the B3LYP/cc-pVDZ Level along with Ionic Radii of M^+ and Corresponding Data for LF, LF^+, and H^+LF

	R_M [a]	R_{MO4}	R_{MN5}	R_{C4O}	α_{N5MO4}	α_{MO4C4}	R_{C2O}	α_{N3C2O2}	ν_{C4O} [b]	ν_{C2O} [b]
LF				1.2155			1.2153	119.1	1740 (245)	1731 (699)
LF^+				1.2067			1.2091	122.1	1752 (146)	1671 (154)
$H^+LF(O4+)$ [d]	0.37	0.985	2.188	1.3055	113.0	107.4	1.2011	116.0	[c]	1789 (788)
$Li^+LF(O4+)$	0.76	1.843	2.085	1.2510	87.8	110.8	1.2051	117.3	1661 (565)	1763 (562)
$Na^+LF(O4+)$	1.02	2.174	2.469	1.2429	73.4	117.7	1.2067	117.8	1670 (533)	1758 (569)
$K^+LF(O4+)$	1.38	2.483	2.935	1.2411	61.4	126.6	1.2076	117.8	1680 (598)	1773 (588)
$Rb^+LF(O4+)$	1.52	2.611	3.126	1.2396	57.5	129.7	1.2080	117.9	1685 (624)	1771 (592)
$Cs^+LF(O4+)$	1.67	2.767	3.401	1.2394	52.8	134.4	1.2083	117.9	1682 (681)	1771 (604)
$Cu^+LF(O4+)$	0.77	2.030	2.009	1.2526	86.5	106.5	1.2047	117.4	1666 (628)	1781 (552)
$Cu^+LF(O4-)$	0.77	2.055	4.767	1.2807	4.5	233.5	1.2056	116.1	[c]	1791 (777)
$Ag^+LF(O4+)$	1.15	2.280	2.339	1.2461	74.8	112.5	1.2056	117.7	1671 (631)	1779 (552)
$Ag^+LF(O4-)$	1.15	2.114	4.803	1.2632	10.0	223	1.2078	116.4	[c]	1783 (759)
$Au^+LF(O4+)$	1.37	2.391	2.222	1.2419	75.0	108.7	1.2051	117.8	1671 (640)	1779 (508)
$Au^+LF(O4-)$	1.37	2.055	4.767	1.2807	4.5	233.7	1.2056	116.1	[c]	1791 (766)
	R_M [a]	R_{MO2}	R_{MN1}	R_{C4O}	α_{N3C2O2}	α_{MO2C2}	R_{C2O}	ν_{C4O} [b]	ν_{C2O} [b]	
$H^+LF(O2+)$ [d]	0.37	0.975	2.30816	1.2025	114.2	108.6	1.3191	1781 (328)	[c]	
$Li^+LF(O2)$	0.76	1.715	3.60413	1.2074	117.1	158.8	1.2673	1763 (320)	1600 (1166)	
$Li^+LF(O2+)$	0.76	1.852	2.08407	1.2048	120.8	92.8	1.2525	1772 (305)	1621 (831)	
$Na^+LF(O2)$	1.02	2.069	3.88681	1.2086	117.5	156.9	1.2571	1759 (320)	1617 (950)	
$Na^+LF(O2+)$	1.02	2.174	2.49780	1.2065	119.4	100.0	1.2456	1767 (310)	1632 (840)	
$K^+LF(O2)$	1.38	2.393	4.27538	1.2092	117.8	162.7	1.2535	1774 (322)	1625 (974)	
$K^+LF(O2+)$	1.38	2.464	3.05549	1.2077	118.7	111.3	1.2456	1779 (320)	1640 (882)	
$Rb^+LF(O2)$	1.52	2.524	4.40569	1.2095	117.8	163.2	1.2512	1773 (324)	1634 (1033)	
$Cs^+LF(O2)$	1.67	2.692	4.57839	1.2097	117.9	164.1	1.2506	1772 (326)	1632 (716)	
$Cu^+LF(O2+)$	0.77	2.082	2.86617	1.2041	121.6	90.2	1.2503	1785 (338)	1574 (369)	
$Cu^+LF(O2-)$	0.77	1.821	4.04778	1.2067	119.9	222.6	1.2826	1782 (328)	1581 (624)	
$Ag^+LF(O2+)$	1.15	2.206	2.61331	1.2054	118.6	102.8	1.2579	1786 (331)	1597 (665)	
$Ag^+LF(O2-)$	1.15	2.095	4.32916	1.2076	120.0	220.6	1.2740	1779 (324)	1586 (682)	
$Au^+LF(O2+)$	1.37	2.065	3.05817	1.2048	114.5	118.2	1.2870	1787 (344)	[c]	
$Au^+LF(O2-)$	1.37	2.037	4.19872	1.2056	121.1	232.7	1.2982	1784 (326)	[c]	

[a]Reference 59. The values are effective ionic radii for the coordination number CN = 6. For H^+, the covalent radius is taken as half of the equilibrium separation of H_2 (0.74 Å). [b]IR intensities (km mol^{-1}) are listed in parentheses. [c]The vibration does not exist as a local mode. [d]Taken from ref 14.

= 23−34 cm^{-1} (32−39 cm^{-1}). LC differs from LF such that it has a proton at N1 but no substituent at N10. In the previously characterized O2 binding site of M^+LC,[15] the alkali ion forms a linear C2═O−M bond. A spherical closed-shell cation should indeed experience an attractive force from both lone pairs of the O2 atom, which is maximized in a linear C2═O−M^+ configuration. In the LF case, the C2═O−M^+ vicinity is less symmetric compared to LC, which also allows for a bent C═O−M^+ arrangement for alkali ions. This is reflected in the corresponding α_{MO2C2} angles for the O2 isomer (Table 3). The C2═O−M^+ angle deviates about 20° from linearity for M^+LF, while a deviation of less than 3° was calculated for the corresponding isomers of M^+LC.[15]

Comparison of the properties of M^+LF with those of bare LF illustrates the effects of metalation at the various binding sites, and the relevant structural and vibrational data computed for LF are available in Table 3. The IR spectrum predicted for bare LF displays two free CO stretch modes at 1731 and 1740 cm^{-1}. Attachment of the M^+ ion to one of the CO groups substantially elongates that bond and reduces the corresponding bound CO stretch frequency in M^+LF, as a result of partial electron transfer from the CO group to the nearby metal ion. At the same time, the remaining free CO stretch frequency increases by a smaller amount because of a minor bond contraction. Comparison of the measured M^+LF spectra with that predicted for bare LF reveals significant red and blue shifts for both CO stretch modes, confirming that the M^+ ion must bind to one of the two available CO groups. This spectral result immediately excludes an assignment to any π complex of M^+LF (such as isomers I and N10), in line with the thermochemical data (Table 1).

With the outlined theoretical analysis, bands A, B1, and B2 can be assigned to the CO stretch modes of the two carbonyl groups of the most stable O2(+) and O4+ isomers of M^+LF by comparison with the computed spectra (Figure 3). Band A is assigned to the overlapping free CO stretch modes, that is, ν_{C2O} of the O4+ isomer and ν_{C4O} of the O2(+) isomers. Bands B1 and B2 are attributed to bound CO stretch modes, that is, ν_{C4O} of the O4+ isomer and ν_{C2O} of the O2(+) isomers. The clear separate observation of the B1 and B2 bands indicates the clear detection of coexisting O2(+) and O4+ isomers for M^+LF with Li−K. Their relative abundance is in accord with their relative energies. Due to the similar spectra predicted for the O2 and O2+ isomers, it is impossible to disentangle their individual contribution to the measured IRMPD spectra at the current spectral resolution. However, because of their small energy difference (<10 kJ/mol), it is likely that both are generated in significant abundance in the electrospray ionization source. In general, the red shifts observed for the bound CO stretches (B1 and B2) increase with the strength of the interaction, that is, with decreasing size of the alkali ion (Table 1, Figure 2). The B2 band is not observed for the Cs^+ case, and the experimental

DOI: 10.1021/acs.jpca.6b08281
J. Phys. Chem. A 2016, 120, 8297−8308

Table 4. NBO Charge Distribution (in me) for Different M^+LF Isomers with Respect to Bare LF Calculated at the B3LYP/cc-pVDZ Level

	q_M	Δq_{O4}	Δq_{N5}	Δq_{O2}
$H^+LF(O4+)$	527	−38	−31	70
$Li^+LF(O4+)$	872	−163	−143	63
$Na^+LF(O4+)$	913	−146	−118	55
$K^+LF(O4+)$	916	−151	−90	49
$Rb^+LF(O4+)$	924	−146	−81	46
$Cs^+LF(O4)$	915	−149	−67	44
$Cu^+LF(O4+)$	784	−115	−153	67
$Cu^+LF(O4-)$	811	−192	19	40
$Ag^+LF(O4+)$	800	−110	−131	62
$Ag^+LF(O4-)$	841	−187	17	36
$Au^+LF(O4+)$	676	−59	−117	68
$Au^+LF(O4-)$	678	−95	23	45
	q_M	Δq_{O2}	Δq_{N5}	Δq_{O4}
$H^+LF(O2+)$	516	−43	40	70
$Li^+LF(O2+)$	880	−145	37	60
Li^+LF (O2)	923	−288	31	45
$Na^+LF(O2+)$	916	−138	33	50
$Na^+LF(O2)$	947	−258	27	48
$K^+LF(O2)$	946	−226	26	35
$K^+LF(O2+)$	930	−153	30	44
$Rb^+LF(O2)$	949	−214	25	33
$Cs^+LF(O2)$	945	−209	24	32
$Cu^+LF(O2+)$	784	12	39	64
$Cu^+LF(O2-)$	796	−197	32	46
$Ag^+LF(O2+)$	803	−122	36	57
$Ag^+LF(O2-)$	833	−198	30	42
$Au^+LF(O2+)$	664	−102	37	62
$Au^+LF(O2-)$	656	−103	34	53

Table 5. Differences in Relative Gibbs Free Energies (kJ/mol), Bond Lengths (pm), and NBO Charge Distributions (in me) of M^+LF and M^+LC[15] Evaluated at the B3LYP/cc-pVDZ Level

	ΔG	ΔR_{MO4}	ΔR_{MN5}	Δq_M	Δq_{O4}	Δq_{N5}
$Li^+LF(O4+) - Li^+LC(O4+)$	4.6	−2.5	2.1	−1	−19	17
$Na^+LF(O4+) - Na^+LC(O4+)$	2.8	−2.7	3.2	1	−18	−19
$K^+LF(O4+) - K^+LC(O4+)$	3.0	−3.6	6.4	1	−22	−51
$Rb^+LF(O4+) - Rb^+LC(O4+)$	3.1	−4.0	7.8	1	−23	−63
$Cs^+LF(O4+) - Cs^+LC(O4+)$	3.7	−4.7	10.4	2	−25	−79
$Cu^+LF(O4+) - Cu^+LC(O4+)$	3.1	−3.3	1.8	1	−18	26
$Ag^+LF(O4+) - Ag^+LC(O4+)$	1.6	−4.2	3.5	2	−20	28
$Au^+LF(O4+) - Au^+LC(O4+)$	−1.3	−8.6	4.8	6	−22	22
	ΔG	ΔR_{MO2}		Δq_M		Δq_{O2}
$Li^+LF(O2) - Li^+LC(O2)$	56.5	−1.3		−9		6
$Na^+LF(O2) - Na^+LC(O2)$	48.3	−1.8		−9		−6
$K^+LF(O2) - K^+LC(O2)$	43.6	−3.5		−9		7
$Rb^+LF(O2) - Rb^+LC(O2)$	41.5	−4.2		−8		6
$Cs^+LF(O2) - Cs^+LC(O2)$	39.3	−5.7		−11		3

Cs^+LF spectrum thus can solely be explained by the presence of the O2 isomer (Figure 3d). Finally, bands C1 and C2 are identified as ring skeleton C−C/C−N stretch vibrations of the observed isomers, denoted as ν_{CN} and ν_{CN}'.

In previous studies, we investigated the influence of alkali ions (Li^+−Cs^+) and a proton on the geometric and electronic structure of LC.[14,15] It was found that the O4+ isomer is the most stable structure of M^+LC for all metal ions investigated. In contrast, the proton binds preferentially to N5 in H^+LC without any interaction with O4. With increasing size of the alkali ion, the energy difference between the O2 and O4+ isomers of M^+LC is reduced due to the decreasing interaction with the N5 lone pair. The energy spacing between both configurations increases roughly linearly with the inverse metal ion radius ($1/R_M$) from 29.1 kJ/mol for Cs^+LC to 67.9 kJ/mol for Li^+LC (Figure 4). Despite these large differences in free

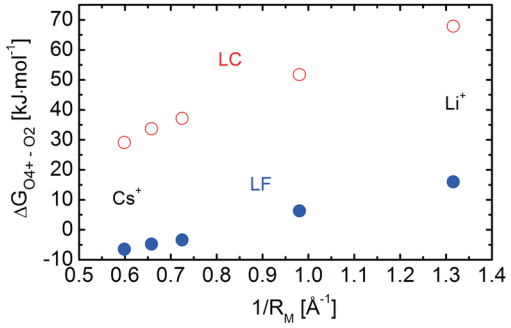

Figure 4. Difference in relative free energies of the O4+ and O2 isomers for M^+LC (open circles) and M^+LF (filled circles) as a function of the inverse ionic radius of the alkali metal ions (Li−Cs) calculated at the B3LYP/cc-pVDZ level.

energy, the O2 isomer could be detected in the M^+LC spectra for M = K−Cs. This situation is in contrast with the M^+LF case, for which the absolute free energy differences between the global minimum and the less stable isomers are smaller than 16 kJ/mol and increase again roughly linearly with $1/R_M$ (Figure 4). However, the O4+ isomer is the most stable isomer for only Li^+LF and Na^+LF. Surprisingly, the O4+ isomer of M^+LF is unambiguously detected for only Li−K, but it could not be resolved for Cs even though the free energy difference between both isomers is predicted to be smaller than 7 kJ/mol for Cs^+LF. It is also interesting to separately compare the binding energies for the O4+ and O2 isomers of M^+LF and M^+LC. Their differences are listed in Table 5, along with relative bond distances and NBO charges. $M^+LF(O4+)$ structures have slightly higher free energies than $M^+LC(O4+)$ by 3−5 kJ/mol. This difference is much larger for the O2 isomers, ranging from 56.5 (Li) to 39.3 kJ/mol (Cs). As a consequence of the energetics, the M−O4 bonds are shorter for $M^+LF(O4+)$ than those for $M^+LC(O4+)$ by $-\Delta R_{MO4}$ = 2.5−4.7 pm, while the M−N5 bond lengths follow the opposite trend (ΔR_{MN5} = 2.1−10.4 pm). Similarly, M^+ is closer to the O2 binding site in $M^+LF(O2)$ as compared to $M^+LC(O2)$ by $-\Delta R_{MO2}$ = 1.3−5.7 pm. The NBO charges on M^+ are essentially the same for both the O4+ (Δq_M = (−1)−2 me) and O2 structures ($-\Delta q_M$ = 9−11 me). The difference in the charges for the binding site is also negligible for the O2 isomers. In contrast, the NBO charges are noticeably higher for both the O4 ($-\Delta q_{O4}$ = 19−25 me) and N5 atoms (Δq_{N5} = 17−(−79) me).

It is instructive to compare the properties of M^+LF with those of the isovalent H^+LF ion characterized previously by the same experimental and computational approach.[14] The proton

DOI: 10.1021/acs.jpca.6b08281
J. Phys. Chem. A 2016, 120, 8297−8308

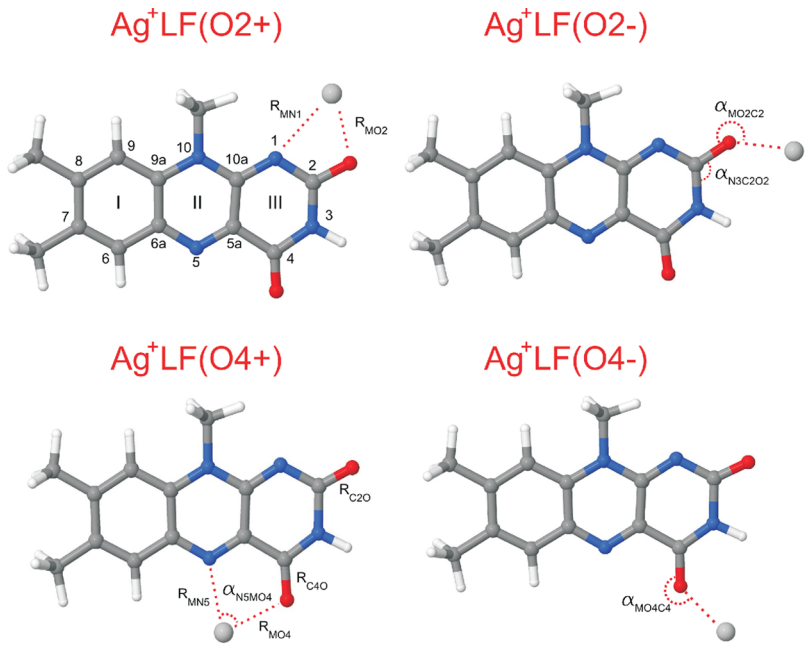

Figure 5. Structures of the planar O2± and O4± isomers of M^+LF complexes with coinage metal cations illustrated for M = Ag, including the atomic and ring numbering (according to IUPAC) and relevant structural parameters.

does not form chelates due to its small size and may bind separately to the nucleophilic O2, N1, O4, or N5 atoms. These isomers (O4+ and N5, O2+ and N1) are separated by appreciable proton transfer barriers. In the most stable H^+LF structure (O2+), which is the only one experimentally detected by IRMPD, the excess proton is located at O2+. The N1, O4+, and N5 protonation sites are 11, 34, and 49 kJ/mol less stable than the O2+ site, respectively.[14] This order of stability (O2+ < N1 < O4+ < N5) does not follow the trend extrapolated here from the small alkali ion series, for which the order is the opposite, namely, O4+ < O2(+). Small alkali ions such as Li and Na are able to form a chelate with N1 and O2. However, the O2+ chelate is less stable than the chelate at the O4+ position. With increasing alkali ion radius, the bonding of the N5−M−O4 chelate becomes weaker, and the O2 position is energetically favored for K−Cs.

3.2. M^+LF with M = Cu, Ag, Au. It is well-known that LF, like any other Fl, does not show any special affinity for transition metal ions in water solution.[8] Closed-shell coinage metal ions have an electronic configuration ($d^{10}s^0$) similar to that of alkali ions (p^6s^0). However, while alkali ions bind mostly by electrostatic and polarization forces, additional orbital interaction of the coinage metal ions arises from sd hybridization ($d^{10-x}s^x$), which leads to enhanced covalent contributions to the M^+−LF bonding. Such orbital interactions have previously been analyzed for Ag^+ binding to pyridine, phenol, cytosine, polycyclic aromatic hydrocarbons, and LC via IR(M)PD spectroscopy and quantum chemical calculations.[15,43,55−57] As the ionization energy calculated for LF (IE = 7.72 eV) is comparable to those of Cu, Ag, and Au (IE = 7.73, 7.58, and 9.23 eV),[54] substantial charge transfer between the coinage metal ions and LF is expected. Depending on the isomer, the charge transfer is calculated as Δq_M = 189−216, 159−200, and 322−344 me for Cu−Au, respectively. According to these numbers, the covalent contribution to the M^+−LF bond increases in the order Ag < Cu < Au. IRMPD spectra have been recorded for Cu^+LF and Ag^+LF, while the generation of Au^+LF in the gas phase via electrospray ionization failed. Nonetheless, the Au^+LF complex is included in the theoretical analysis for completeness.

The same four low-energy binding motifs shown in Figure 5 emerge for M^+LF with all three coinage metals (Tables 1, 3, and 4). Similar to the small and strongly bonded alkali metals Li and Na, the calculations reveal that the σ-bonded planar O4+ structures with an N5−M−O4 chelate are the most stable isomers for all coinage metals, with Gibbs free energies of 350, 262, and 321 kJ/mol for Cu, Ag, and Au, respectively. Interestingly, there is a second O4− minimum, in which M^+ binds away from N5. No such stable O4− isomers are predicted for alkali ions. These O4− isomers are considerably less stable than the O4+ global minima (by 76, 60, 52 kJ/mol for Cu−Au) because they lack the M^+−N5 interaction. The M^+LF(O2+) isomers are less stable than the O4+ global minima (by 26, 3, 2 kJ/mol for Cu−Au), and again, the O2− isomers are substantially less stable than the O2+ isomers (by 24, 35, 25 kJ/mol for Cu−Au) because they lack the M^+−N1 interaction. This bent bonding behavior in the O2− isomers is different from that of the alkali ions, which prefer (nearly) linear bonds when forming the O2 isomer. One reason for the existence of the O2− (O4−) binding site is the d orbital electronic structure of the coinage metal ions and the resulting $d^{10-x}s^x$ hybridization. This leads to a preferred bent C═O−M^+ configuration, with covalent bonding of one d_zs orbital of M^+ with one lone pair of C═O. The angles for the two bent C2═O−M^+ configurations O2+ and O2− (O4+ and O4−) differ due to the additional bonding to N1 (N5) for the O2+ (O4+) isomer (Table 3). These interactions also explain the difference in Gibbs energy of the O2+ and O2− isomers. The search for π complexes for Cu and Ag yields a stable minimum, in which the coinage metal ion forms a covalent bond to the C9 atom of the benzene ring,[56,57] denoted M^+LF(I). However, this C-bonded isomer has a significantly lower binding free energy than the O4+ global minimum (by 164 and 151 kJ/mol for Cu and Ag). No other C-bound structure has been found. In general, the

DOI: 10.1021/acs.jpca.6b08281
J. Phys. Chem. A 2016, 120, 8297−8308

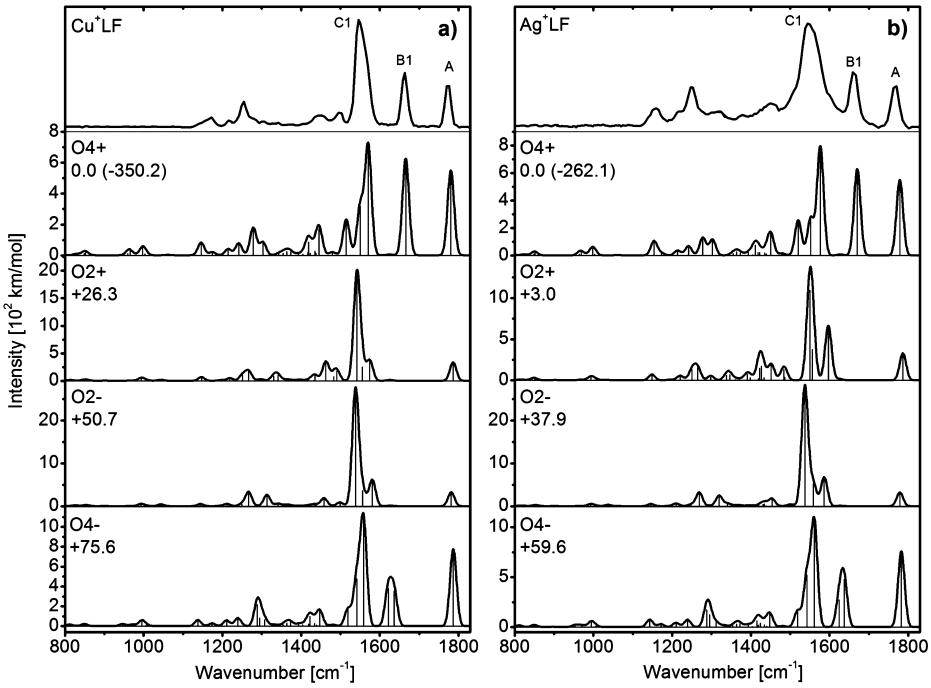

Figure 6. Experimental IRMPD spectra of M^+LF complexes with the coinage metals Cu (a) and Ag (b) compared to the linear IR absorption spectra calculated for the lowest-energy isomers (B3LYP/cc-pVDZ). Calculated stick spectra are convoluted with a Gaussian line profile with fwhm = 20 cm^{-1}. Relative (absolute) free energies for the global (local) minima are given in kJ/mol.

additional covalent contributions to the M^+LF bonding for the coinage metals leads to higher binding energies than those for the alkali ions, which can clearly be evidenced in the plot of the binding energy versus the inverse ionic radius (Figure S9 in the SI). For example, even though Ag^+ has a much larger ionic radius than Li^+ (1.15 and 0.76 Å), their M^+LF binding energies are comparable. Along the same line, Cu^+ and Li^+ have similar ionic radii (0.77 and 0.76 Å), but the Cu^+LF bonds are much stronger than those of Li^+LF.

The measured IRMPD spectra of Cu^+LF and Ag^+LF are compared in Figure 6 to linear IR spectra calculated for the O2± and O4± isomers, and their relevant energetic, structural, and vibrational properties as well as the charge distributions are summarized in Tables 1, 3, and 4 and Figures S9−S11 in the SI. While the O4+ and O4− spectra are clearly different due to the additional M^+−N5 interaction in the former isomer, the spectra of the O2± isomers are similar in the considered fingerprint range. The spectra predicted for the M^+LF(I) isomers are different because this type of isomer has two free CO bonds and no M^+−O interaction (Figures S6 and S7 in the SI). Closer inspection of Figure 6 reveals a good match between the IRMPD spectra of M^+LF and the IR spectra predicted for the most stable O4+ isomer, in particular with respect to the positions and relative intensities of bands A, B1, and C1. Although there is no clear-cut spectroscopic signature for the less stable isomers in the IRMPD spectra, their minor contribution cannot be ruled out completely. For example, the relatively stable O2+ local minimum of Ag^+LF may contribute as a blue shoulder to band C near 1550 cm^{-1}.

Despite the similar binding energies for Ag^+LF(O4+) and Li^+LF(O4+), the measured IRMPD spectra are quite different from each other (Figure 2). For Ag^+LF, mainly the O4+ isomer is present (with a possible minor contamination of O2+), while the O4+ and O2(+) isomers are clearly identified with similar abundance for Li^+LF by the presence of bands B1 and B2 even though the energy difference to the second most stable O2+ isomer is comparable (+7.2 kJ/mol for Li, +3.0 kJ/mol for Ag). This is in contrast with what is found for the Li^+LC and Ag^+LC complexes,[15] for which the spectra are practically identical and for which only the M^+LC(O4+) isomer is identified. In the case of the M^+LC complexes, the high relative energies of the O2 conformers of M^+LC (+67.9 kJ/mol for Li and +86.1 kJ/mol for Ag) prevent their formation in the electrospray ionization source. On the other hand, the absence (or at most minor abundance) of the Ag^+LF(O2+) isomer under the same experimental conditions is unexpected and remains to be explained.

4. CONCLUDING REMARKS

The formation of metal−organic complexes of LF with a variety of metal ions has been studied by IRMPD spectroscopy and quantum chemical calculations of mass-selected isolated M^+LF complexes generated by electrospray ionization. Significantly, these are the first spectroscopic data obtained for M^+LF complexes in the gas phase and thus provide a first impression of the M^+−LF interaction free from perturbation by solvent molecules and counterions. The preferred binding site, strength, and type of interaction have systematically been characterized for two types of metal ions, namely, alkali and coinage metals (Li^+−Cs^+, Cu^+−Au^+) to probe the dependence of the interaction on the type and size of the metal ion. The CO stretch frequencies of the two carbonyl groups of LF provide a sensitive indicator of the metal binding site and bond strength in M^+LF because these are the most attractive M^+ binding sites. Computationally, the O4+ structure is identified as the most stable isomer for the small alkali (Li, Na) and all coinage metal ions, which feature the strongest M^+−LF bonds. In contrast, the O2 isomer is predicted to be the global minimum for the larger alkali ions (K−Cs) with weaker M^+−LF interaction. In the O4+ configuration, the metal ion

DOI: 10.1021/acs.jpca.6b08281
J. Phys. Chem. A 2016, 120, 8297−8308

benefits from the formation of a N5−M−O4 chelate stabilized by interactions with the lone pairs of both N5 and O4 of LF. The O2 isomers lack a similar stabilizing interaction with N1, leading to smaller binding energies for Li, Na, and Cu−Au. Nonetheless, this isomer is identified in the M^+LF spectra with M = K−Cs, and it is, in fact, the most stable one for these alkali metals. This result is due to the reduced M^+−N5 interaction for the larger alkali ions. For the alkali ions, all energetic, structural, electronic, and vibrational parameters of M^+LF scale monotonically and roughly linearly with the inverse ionic radius of M^+. This behavior is rationalized by the dominant electrostatic and induction contributions to the attractive part of the interaction potential. In contrast, the coinage metal ions deviate in many aspects from this trend due to the additional covalent contributions to the bonding, which are smallest for Ag^+ and quite substantial for Cu^+ and Au^+. These covalent contributions also influence the geometries of the binding motifs (e.g., O2− and O4− only exist for the coinage metal ions). Significantly, all M^+LF structures differ from that of H^+LF, which prefers protonation at the C2O group in a O2+ configuration.[14] Moreover, comparison between M^+LF and M^+LC reveals large implications of methylation of N10 and simultaneous dehydrogenation of N1 on the M^+−Fl interaction potential. This is particularly pronounced in the vicinity of the O2 binding site because of the (non)availability of the N1−M^+ interaction. However, also the O4+ isomers of M^+LF have slightly lower binding energies than their corresponding M^+LC counterparts by a few kJ/mol, as a result of the different geometric and electronic structures of the pyridine and pyrimidine rings of the two Fls. The charge transfer in M^+LF should be mostly localized on the n orbitals of LF, whereas the electronic structure of the aromatic π electron system is expected to be less affected. Consequently, electronic $\pi \rightarrow \pi^*$ transitions may be less affected by metalation, whereas the $n \rightarrow \pi^*$ transitions may show larger changes in their position, coupling, and lifetime. In the future, we will explore the optical spectra of these M^+Fl complexes to probe the effects of metal complexation on the electronic structure of the Fl chromophore in these fundamental complexes.[58]

■ ASSOCIATED CONTENT

Supporting Information

The Supporting Information is available free of charge on the ACS Publications website at DOI: 10.1021/acs.jpca.6b08281.

Laser power curves of FELIX; structures of the I and N10 isomers of Li^+LF; calculated linear IR absorption spectra of all M^+LF isomers; free energies, charges, and selected structural and vibrational parameters plotted as a function of the inverse ionic radius of the metal; and fragment ion channels used to monitor the IRMPD spectra (PDF)

■ AUTHOR INFORMATION

Corresponding Author

*E-mail: dopfer@physik.tu-berlin.de. Phone: +49 30 314 23017. Fax: +49 30 314 23018.

Notes

The authors declare no competing financial interest.

■ ACKNOWLEDGMENTS

This work was supported by the Deutsche Forschungsgemeinschaft (DO 729/6). The research leading to these results received funding from the European Community's Seventh Framework Program (FP7/2007-2013) under Grant Agreement Number 226716. This work is part of the research program of FOM, which is financially supported by the Nederlandse Organisatie voor Wetenschappelijk Onderzoek (NWO). We gratefully acknowledge the excellent assistance by the FELIX staff. We thank Judith Langer and Sophie Seidenbecher for assistance in the initial experimental and computational data acquisition.

■ REFERENCES

(1) Heelis, P. F. The Photophysical and Photochemical Properties of Flavins. *Chem. Soc. Rev.* **1982**, *11*, 15−39.

(2) *Flavins: Photochemistry and Photobiology*; Silva, E., Edwards, A. M., Eds.; Comprehensive series in photochemistry and photobiology; RSC Pub: Cambridge, U.K., 2006; Vol. *6*.

(3) Rutter, W. J.; Dalziel, K.; Viervoll, H.; Zackrisson, M.; Ernster, L.; Diczfalusy, E. The Interaction of Riboflavin, FMN, and FAD with Various Metal Ions: The Riboflavin Catalyzed Photochemical Reduction of Fe^{III}, and Photooxidation of Fe^{II}. *Acta Chem. Scand.* **1958**, *12*, 438−446.

(4) Benecky, M.; Yu, T. Y.; Watters, K. L.; McFarland, J. T. Metal-Flavin Complexation. A Resonance Raman Investigation. *Biochim. Biophys. Acta, Protein Struct.* **1980**, *626*, 197−207.

(5) Lauterwein, J.; Hemmerich, P.; Lhoste, J. M. Flavoquinone-Metal Complexes. I. Structure and Properties. *Inorg. Chem.* **1975**, *14*, 2152−2161.

(6) Lauterwein, J.; Hemmerich, P.; Lhoste, J. M. Flavoquinone-Metal Complexes. II. Paramagnetic Interactions. *Inorg. Chem.* **1975**, *14*, 2161−2168.

(7) Muller, F.; Hemmerich, P.; Ehrenberg, A. Light Absorption of Flavosemiquinone Metal Chelates. *Eur. J. Biochem.* **1968**, *5*, 158−164.

(8) Hemmerich, P.; Lauterwein, J. The Structure and Reactivity of Flavin-Metal Complexes. In *Inorganic Biochemistry*; Eichhorn, G. L., Ed.; Elsevier Scientific Pub. Co: Amsterdam, London, New York, 1973; Vol. *2*.

(9) Losi, A.; Gärtner, W. Old Chromophores, New Photoactivation Paradigms, Trendy Applications: Flavins in Blue Light-Sensing Photoreceptors. *Photochem. Photobiol.* **2011**, *87*, 491−510.

(10) Swartz, T. E.; Tseng, T. S.; Frederickson, M. A.; Paris, G.; Comerci, D. J.; Rajashekara, G.; Kim, J. G.; Mudgett, M. B.; Splitter, G. A.; Ugalde, R. A.; et al. Blue-Light-Activated Histidine Kinases: Two-Component Sensors in Bacteria. *Science* **2007**, *317*, 1090−1093.

(11) Sugiyama, M. Effects of Vitamins on Chromium(VI)-Induced Damage. *Environ. Health Persp.* **1991**, *92*, 63−70.

(12) Massey, V. The Chemical and Biological Versatility of Riboflavin. *Biochem. Soc. Trans.* **2000**, *28*, 283−296.

(13) Hasegawa, J.; Bureekaew, S.; Nakatsuji, H. SAC-CI Theoretical Study on the Excited States of Lumiflavin: Structure, Excitation Spectrum, and Solvation Effect. *J. Photochem. Photobiol., A* **2007**, *189*, 205−210.

(14) Langer, J.; Günther, A.; Seidenbecher, S.; Berden, G.; Oomens, J.; Dopfer, O. Probing Protonation Sites of Isolated Flavins Using IR Spectroscopy: From Lumichrome to the Cofactor Flavin Mononucleotide. *ChemPhysChem* **2014**, *15*, 2550−2562.

(15) Günther, A.; Nieto, P.; Berden, G.; Oomens, J.; Dopfer, O. IRMPD Spectroscopy of Metalated Flavins: Structure and Bonding of M^{q+}-Lumichrome Complexes (M^{q+} = Li^+−Cs^+, Ag^+, Mg^{2+}). *Phys. Chem. Chem. Phys.* **2014**, *16*, 14161−14171.

(16) Zhang, T.; Papson, K.; Ochran, R.; Ridge, D. P. Stability of Flavin Semiquinones in the Gas Phase: The Electron Affinity, Proton Affinity, and Hydrogen Atom Affinity of Lumiflavin. *J. Phys. Chem. A* **2013**, *117*, 11136−11141.

(17) Vdovin, A.; Slenczka, A.; Dick, B. Electronic Spectroscopy of Lumiflavin in Superfluid Helium Nanodroplets. *Chem. Phys.* **2013**, *422*, 195−203.

(18) Guyon, L.; Tabarin, T.; Thuillier, B.; Antoine, R.; Broyer, M.; Boutou, V.; Wolf, J. P.; Dugourd, P. Femtosecond Pump-Probe

DOI: 10.1021/acs.jpca.6b08281
J. Phys. Chem. A 2016, 120, 8297−8308

Experiments on Trapped Flavin: Optical Control of Dissociation. *J. Chem. Phys.* **2008**, *128*, 075103.
(19) Lagutschenkov, A.; Langer, J.; Berden, G.; Oomens, J.; Dopfer, O. Infrared Spectra of Protonated Neurotransmitters: Serotonin. *J. Phys. Chem. A* **2010**, *114*, 13268−13276.
(20) Lagutschenkov, A.; Langer, J.; Berden, G.; Oomens, J.; Dopfer, O. Infrared Spectra of Protonated Neurotransmitters: Dopamine. *Phys. Chem. Chem. Phys.* **2011**, *13*, 2815−2823.
(21) Lagutschenkov, A.; Springer, A.; Lorenz, U. J.; Maitre, P.; Dopfer, O. Structure of Zirconocene Complexes Relevant for Olefin Catalysis: Infrared Fingerprint of the $Zr(C_5H_5)_2(OH)(CH_3CN)^+$ Cation in the Gas Phase. *J. Phys. Chem. A* **2010**, *114*, 2073−2079.
(22) Chiavarino, B.; Crestoni, M. E.; Schutz, M.; Bouchet, A.; Piccirillo, S.; Steinmetz, V.; Dopfer, O.; Fornarini, S. Cation-π Interactions in Protonated Phenylalkylamines. *J. Phys. Chem. A* **2014**, *118*, 7130−7138.
(23) Chiavarino, B.; Crestoni, M. E.; Dopfer, O.; Maitre, P.; Fornarini, S. Benzylium versus Tropylium Ion Dichotomy: Vibrational Spectroscopy of Gaseous $C_8H_9^+$ Ions. *Angew. Chem., Int. Ed.* **2012**, *51*, 4947−4949.
(24) Chiavarino, B.; Crestoni, M. E.; Fornarini, S.; Dopfer, O.; Lemaire, J.; Maitre, P. IR Spectroscopic Features of Gaseous $C_7H_7O^+$ Ions: Benzylium versus Tropylium Ion Structures. *J. Phys. Chem. A* **2006**, *110*, 9352−9360.
(25) Dopfer, O.; Lemaire, J.; Maître, P.; Chiavarino, B.; Crestoni, M. E.; Fornarini, S. IR Spectroscopy of Protonated Toluene: Probing Ring Hydrogen Shifts in Gaseous Arenium Ions. *Int. J. Mass Spectrom.* **2006**, *249*−*250*, 149−154.
(26) Bouchet, A.; Schutz, M.; Dopfer, O. Competing Insertion and External Binding Motifs in Hydrated Neurotransmitters: Infrared Spectra of Protonated Phenylethylamine Monohydrate. *ChemPhysChem* **2016**, *17*, 232−243.
(27) Bouchet, A.; Klyne, J.; Piani, G.; Dopfer, O.; Zehnacker, A. Diastereo-Specific Conformational Properties of Neutral, Protonated and Radical Cation Forms of (1R,2S)-cis- and (1R,2R)-trans-Amino-Indanol by Gas Phase Spectroscopy. *Phys. Chem. Chem. Phys.* **2015**, *17*, 25809−25821.
(28) Fridgen, T. D. Infrared Consequence Spectroscopy of Gaseous Protonated and Metal Ion Cationized Complexes. *Mass Spectrom. Rev.* **2009**, *28*, 586−607.
(29) Polfer, N. C.; Oomens, J. Vibrational Spectroscopy of Bare and Solvated Ionic Complexes of Biological Relevance. *Mass Spectrom. Rev.* **2009**, *28*, 468−494.
(30) Eyler, J. R. Infrared Multiple Photon Dissociation Spectroscopy of Ions in Penning Traps. *Mass Spectrom. Rev.* **2009**, *28*, 448−467.
(31) Seydou, M.; Gregoire, G.; Liquier, J.; Lemaire, J.; Schermann, J. P.; Desfrancois, C. Experimental Observation of the Transition between Gas-Phase and Aqueous Solution Structures for Acetylcholine, Nicotine, and Muscarine Ions. *J. Am. Chem. Soc.* **2008**, *130*, 4187−4195.
(32) MacAleese, L.; Maitre, P. Infrared Spectroscopy of Organometallic Ions in the Gas Phase: from Model to Real World Complexes. *Mass Spectrom. Rev.* **2007**, *26*, 583−605.
(33) Dopfer, O. IR Spectroscopic Strategies for the Structural Characterization of Isolated and Microsolvated Arenium Ions. *J. Phys. Org. Chem.* **2006**, *19*, 540−551.
(34) Oomens, J.; Sartakov, B. G.; Meijer, G.; von Helden, G. Gas-Phase Infrared Multiple Photon Dissociation Spectroscopy of Mass-Selected Molecular Ions. *Int. J. Mass Spectrom.* **2006**, *254*, 1−19.
(35) Lorenz, U. J.; Solca, N.; Lemaire, J.; Maitre, P.; Dopfer, O. Infrared Spectra of Isolated Protonated Polycyclic Aromatic Hydrocarbons: Protonated Naphthalene. *Angew. Chem., Int. Ed.* **2007**, *46*, 6714−6716.
(36) Knorke, H.; Langer, J.; Oomens, J.; Dopfer, O. Infrared Spectra of Isolated Protonated Polycyclic Aromatic Hydrocarbon Molecules. *Astrophys. J.* **2009**, *706*, L66−L70.
(37) Dopfer, O.; Solca, N.; Lemaire, J.; Maitre, P.; Crestoni, M. E.; Fornarini, S. Protonation Sites of Isolated Fluorobenzene Revealed by IR Spectroscopy in the Fingerprint Range. *J. Phys. Chem. A* **2005**, *109*, 7881−7887.
(38) Lorenz, U. J.; Lemaire, J.; Maitre, P.; Crestoni, M. E.; Fornarini, S.; Dopfer, O. Protonation of Heterocyclic Aromatic Molecules: IR Signature of the Protonation Site of Furan and Pyrrole. *Int. J. Mass Spectrom.* **2007**, *267*, 43−53.
(39) Zhao, D.; Langer, J.; Oomens, J.; Dopfer, O. Infrared Spectra of Protonated Polycyclic Aromatic Hydrocarbon Molecules: Azulene. *J. Chem. Phys.* **2009**, *131*, 184307.
(40) *Gas-Phase IR Spectroscopy and Structure of Biological Molecules*; Rijs, M. A., Oomens, J., Eds.; Springer International Publishing: Cham, Switzerland, 2015.
(41) Lagutschenkov, A.; Lorenz, U. J.; Dopfer, O. IR Spectroscopy of Isolated Metal−Organic Complexes of Biocatalytic Interest: Evidence for Coordination Number Four for $Zn^{2+}(Imidazole)_4$. *Int. J. Mass Spectrom.* **2011**, *308*, 316−329.
(42) Boles, G. C.; Coates, R. A.; Berden, G.; Oomens, J.; Armentrout, P. B. Experimental and Theoretical Investigations of Infrared Multiple Photon Dissociation Spectra of Glutamine Complexes with Zn^{2+} and Cd^{2+}. *J. Phys. Chem. B* **2015**, *119*, 11607−11617.
(43) Gao, J.; Berden, G.; Rodgers, M. T.; Oomens, J. Interaction of Cu^+ with Cytosine and Formation of i-Motif-Like C-M^+-C Complexes: Alkali versus Coinage Metals. *Phys. Chem. Chem. Phys.* **2016**, *18*, 7269−7277.
(44) Yang, B.; Wu, R. R.; Polfer, N. C.; Berden, G.; Oomens, J.; Rodgers, M. T. IRMPD Action Spectroscopy of Alkali Metal Cation-Cytosine Complexes: Effects of Alkali Metal Cation Size on Gas Phase Conformation. *J. Am. Soc. Mass Spectrom.* **2013**, *24*, 1523−1533.
(45) Dunbar, R. C.; Steill, J. D.; Polfer, N. C.; Berden, G.; Oomens, J. Peptide Bond Tautomerization Induced by Divalent Metal Ions: Characterization of the Iminol Configuration. *Angew. Chem., Int. Ed.* **2012**, *51*, 4591−4593.
(46) Coates, R. A.; McNary, C. P.; Boles, G. C.; Berden, G.; Oomens, J.; Armentrout, P. B. Structural Characterization of Gas-Phase Cysteine and Cysteine Methyl Ester Complexes with Zinc and Cadmium Dications by Infrared Multiple Photon Dissociation Spectroscopy. *Phys. Chem. Chem. Phys.* **2015**, *17*, 25799−25808.
(47) Cole, R. B. *Electrospray Mass Spectrometry: Fundamentals, Instrumentation, and Applications*, 2nd ed.; Wiley-Blackwell: Oxford, U.K., 2008.
(48) Valle, J. J.; Eyler, J. R.; Oomens, J.; Moore, D. T.; van der Meer, A. F. G.; von Helden, G.; Meijer, G.; Hendrickson, C. L.; Marshall, A. G.; Blakney, G. T. Free Electron Laser-Fourier Transform Ion Cyclotron Resonance Mass Spectrometry Facility for Obtaining Infrared Multiphoton Dissociation Spectra of Gaseous Ions. *Rev. Sci. Instrum.* **2005**, *76*, 023103.
(49) Oepts, D.; van der Meer, A. F. G.; van Amersfoort, P. W. The Free-Electron-Laser User Facility FELIX. *Infrared Phys. Technol.* **1995**, *36*, 297−308.
(50) Frisch, M. J.; Trucks, G. W.; Schlegel, H. B.; Scuseria, G. E.; Robb, M. A.; Cheeseman, J. R.; Scalmani, G.; Barone, V.; Mennucci, B.; Petersson, G. A.; et al. *Gaussian 09*, revision D.01; Gaussian, Inc.: Wallingford, CT, 2009.
(51) Hay, P. J.; Wadt, W. R. Ab Initio Effective Core Potentials for Molecular Calculations. Potentials for the Transition Metal Atoms Sc to Hg. *J. Chem. Phys.* **1985**, *82*, 270−283.
(52) Parneix, P.; Basire, M.; Calvo, F. Accurate Modeling of Infrared Multiple Photon Dissociation Spectra: The Dynamical Role of Anharmonicities. *J. Phys. Chem. A* **2013**, *117*, 3954−3959.
(53) Reed, A. E.; Curtiss, L. A.; Weinhold, F. Intermolecular Interactions from a Natural Bond Orbital, Donor-Acceptor Viewpoint. *Chem. Rev.* **1988**, *88*, 899−926.
(54) Linstrom, P. J., Mallard, W. G., Eds. *NIST Chemistry WebBook*, NIST Standard Reference Database Number 69. National Institute of Standards and Technology: Gaithersburg, MD. http://webbook.nist.gov (Accessed August 16, 2016).
(55) Chakraborty, S.; Dopfer, O. Infrared Spectrum of the Ag^+−$(Pyridine)_2$ Ionic Complex: Probing Interactions in Artificial Metal-Mediated Base Pairing. *ChemPhysChem* **2011**, *12*, 1999−2008.

DOI: 10.1021/acs.jpca.6b08281
J. Phys. Chem. A 2016, 120, 8297−8308

(56) Lagutschenkov, A.; Sinha, R. K.; Maitre, P.; Dopfer, O. Structure and Infrared Spectrum of the Ag^+−Phenol Ionic Complex. *J. Phys. Chem. A* **2010**, *114*, 11053−11059.
(57) Savoca, M.; Wende, T.; Jiang, L.; Langer, J.; Meijer, G.; Dopfer, O.; Asmis, K. R. Infrared Spectra and Structures of Silver−PAH Cation Complexes. *J. Phys. Chem. Lett.* **2011**, *2*, 2052−2056.
(58) Günther, A.; Nieto, P.; Müller, D.; Sheldrick, A.; Gerlich, D.; Dopfer, O. BerlinTrap: A New Cryogenic 22-Pole Ion Trap Spectrometer. *J. Mol. Spectrosc.* **2016**, DOI: 10.1016/j.jms.2016.08.017.
(59) Shannon, R. D. Revised Effective Ionic Radii and Systematic Studies of Interatomic Distances in Halides and Chalcogenides. *Acta Crystallogr., Sect. A: Cryst. Phys., Diffr., Theor. Gen. Crystallogr.* **1976**, *32*, 751−767.

DOI: 10.1021/acs.jpca.6b08281
J. Phys. Chem. A 2016, 120, 8297−8308